Published in final edited form as:
Neuroscience. 2011 March 31; 178: 21–32. doi:10.1016/j.neuroscience.2011.01.020.

Laminar-specific and developmental expression of aquaporin-4 in the mouse hippocampus

Mike S. Hsu[1], **Marcus Seldin**[2], **Darrin J. Lee**[3], **Gerald Seifert**[4], **Christian Steinhäuser**[4], and **Devin K. Binder**[1]

[1]Center for Glial-Neuronal Interactions, Division of Biomedical Sciences University of California, Riverside, CA, USA

[2]Department of Physiology, Johns Hopkins University, Baltimore, MD, USA

[3]Department of Neurological Surgery, University of California, Davis, CA, USA

[4]Institute of Cellular Neurosciences, University of Bonn, Bonn, Germany

Abstract

Mice deficient in the water channel AQP4 demonstrate increased seizure duration in response to hippocampal stimulation as well as impaired extracellular K^+ clearance. However, the expression of AQP4 in the hippocampus is not well described. In this study, we investigated i) the developmental, laminar and cell-type specificity of AQP4 expression in the hippocampus; ii) the effect of $K_{ir}4.1$ deletion on AQP4 expression; and iii) performed Western blot and RT-PCR analyses. AQP4 immunohistochemistry on coronal sections from WT or $K_{ir}4.1^{-/-}$ mice revealed a developmentally-regulated and laminar-specific pattern, with highest expression in the CA1 stratum lacunosummoleculare (SLM) and the molecular layer (ML) of the dentate gyrus (DG). AQP4 was colocalized with the glial markers GFAP and S100ß in the hippocampus, and was also ubiquitously expressed on astrocytic endfeet around blood vessels. No difference in AQP4 immunoreactivity was observed in $K_{ir}4.1^{-/-}$ mice. Electrophysiological and postrecording RT-PCR analyses of individual cells revealed that AQP4 and $K_{ir}4.1$ were co-expressed in nearly all CA1 astrocytes. In NG2 cells, AQP4 was also expressed at the transcript level. This study is the first to examine subregional AQP4 expression during development of the hippocampus. The strikingly high expression of AQP4 in the CA1 SLM and DG ML identifies these regions as potential sites of astrocytic K^+ and H_2O regulation. These results begin to delineate the functional capabilities of hippocampal subregions and cell types for K^+ and H_2O homeostasis, which is critical to excitability and serves as a potential target for modulation in diverse diseases.

Keywords

aquaporin; astrocyte; glial cell; potassium; water

Corresponding author: Devin K. Binder, M.D., Ph.D. Center for Glial-Neuronal Interactions Division of Biomedical Sciences 1247 Webber Hall University of California, Riverside Riverside, CA 92521-0121 Tel: 951-827-2224 Fax: 951-827-5504 dbinder@ucr.edu.

INTRODUCTION

The aquaporins (AQPs) are a family of membrane proteins that function as “water channels” in many cell types and tissues in which fluid transport is crucial (Verkman, 2005). There is increasing evidence that water movement in the brain involves aquaporin channels (Amiry-Moghaddam and Ottersen, 2003). Aquaporin-4 (AQP4) is expressed ubiquitously by glial cells throughout the brain, especially at specialized membrane domains including astroglial endfeet in contact with blood vessels and astrocyte membranes that ensheathe glutamatergic synapses (Nielsen et al., 1997, Nagelhus et al., 2004). Activity-induced radial water fluxes in neocortex have been demonstrated that could be due to water movement via aquaporin channels in response to physiological activity (Niermann et al., 2001). Mice deficient in AQP4 (AQP4$^{-/-}$ mice) have markedly decreased accumulation of brain water (cerebral edema) following water intoxication and focal cerebral ischemia (Manley et al., 2000) and impaired clearance of brain water in models of vasogenic edema (Papadopoulos et al., 2004), suggesting a functional role for AQP4 in brain water transport. Similarly, mice deficient in dystrophin or α-syntrophin, in which there is mislocalization of the AQP4 protein (Frigeri et al., 2001, Neely et al., 2001, Vajda et al., 2002), also demonstrate attenuated cerebral edema (Vajda et al., 2002, Amiry-Moghaddam et al., 2003). In addition, RNAi knockdown of AQP4 impairs brain water mobility (Badaut et al., 2010).

In previous studies, AQP4$^{-/-}$ mice have also been shown to have expanded brain extracellular space (Binder et al., 2004, Yao et al., 2008), and also significant alterations in neural excitability, with a three-fold increase in hippocampal stimulation-induced seizure duration and impaired potassium homeostasis (Binder et al., 2006, Hsu et al., 2007). However, the expression of AQP4 in the hippocampus, a structure critical to excitability and seizures, has not yet been described in detail. Furthermore, the expression and role of AQP4 and the inwardly-rectifying potassium channel $K_{ir}4.1$ (a putative molecular partner in K^+ homeostasis) in subsets of hippocampal glial cells are still unclear. In this study, we examine the developmental, laminar-specific, and cell type-specific expression of AQP4 in the mouse hippocampus with immunohistochemistry; examine the effect of $K_{ir}4.1$ deletion on AQP4 expression; and use single-cell reverse transcription (RT)-PCR analysis to examine transcript levels of AQP4 and $K_{ir}4.1$ in identified astrocytes and NG2 glia.

EXPERIMENTAL PROCEDURES

Mice

Male CD1 mice at various ages were used (n=20 WT, 20 AQP4$^{-/-}$). AQP4$^{-/-}$ mice were generated as previously described (Ma et al., 1997). These mice lack detectable AQP4 protein and phenotypically have normal growth, development, survival, and neuromuscular function. Sections from AQP4$^{-/-}$ mice were used as controls to optimize the sensitivity and specificity of our immunohistochemistry. $K_{ir}4.1^{-/-}$ mice were a kind gift from P. Kofuji (Kofuji et al., 2000). As this mutation leads to early postnatal death, we examined only P9 tissue from $K_{ir}4.1^{-/-}$ mice. For patch clamp and RT-PCR analyses, transgenic hGFAP/EGFP mice were used (Nolte et al., 2001).

AQP4 immunohistochemistry

Mice of age P9, 3 weeks, and 6 weeks were anaesthetized with sodium pentobarbital and perfused transcardially with 2% paraformaldehyde (pH 7.4) in phosphate-buffered saline (PBS). Brains were dissected, postfixed overnight in perfusion buffer, cryoprotected in 30% sucrose/PBS, frozen in isopentane, and then 50 μm coronal sections were cut on a cryostat (Leica 1910, Leica Microsystems, Bannockburn, IL). Briefly, floating sections were quenched in 3% peroxide/PBS for 1 hr, blocked for nonspecific binding in 5% NGS/PBS in

1 hr, and incubated overnight at 4°C with primary antibody (1:200 rabbit polyclonal anti-aquaporin-4, AB3068, Chemicon, Temecula, CA) in 0.3% Triton X-100/PBS. After extensive washing in PBS, sections were incubated with secondary antibody (1:100 anti-rabbit IgG conjugated to HRP, G21234, Invitrogen) for 30 minutes, washed, then developed with Alexa Fluor 488-conjugated tyramide (1:100, T-20922, Invitrogen) for 10 min, washed, counterstained with fluorescent Neurotrace nissl dye (1:10, N21479, Invitrogen) for 10 min, mounted on frosted slides (Fisher), dried, and coverslipped with Vectashield (Vector laboratories). Sections from AQP4$^{-/-}$ mice were used as controls to optimize the assay. K_{ir}4.1 staining in wild-type (WT) and AQP4$^{-/-}$ tissue followed the same protocol as detailed above, except rabbit anti-K_{ir}4.1 (1:200, APC-035, Alomone, Jerusalem, Israel) was used as the primary antibody as previously described (Seifert et al., 2009). Images were obtained using a fluorescence microscope (BX-51, Olympus America, Center Valley, PA) and data obtained from images were analyzed using Slidebook software (3I). For confocal analysis, images were obtained using a Carl Zeiss LSM510 Meta (Carl Zeiss North America, Thornwood, NY).

Multiple immunofluorescence detection of AQP4 with other neuronal and glial markers were carried out using a modified protocol with alternative primary and fluorescent secondary antibodies. Sections were incubated, in addition to AQP4, with mouse anti-NeuN (1:100, MAB377, Chemicon), mouse anti-GFAP (1:100, MAB360, Chemicon), and anti-S-100β (1:1000, Swiss Antibodies, Bellinzona, Switzerland), rabbit anti-K_{ir}4.1 (1:200, APC-035, Alomone). Double immunofluorescence labeling of AQP4 with NG2 was carried out by incubating with polyclonal goat anti-AQP4 (1:40, Santa Cruz) and rabbit anti-NG2 (1:100, Chemicon) primary antibodies. Following tyramide development, sections were incubated with the species-appropriate Alexa Fluor 594-conjugated secondary antibody (1:100, Invitrogen) for 2 hours at RT.

Western blot analysis

For Western blot analysis, brain tissue from animals of age P9, 3 weeks, and 6 weeks was used (n=3 per time point). Mice were perfused transcardially with ice-cold PBS and brains were removed. Western blots were performed on protein extracted from homogenates of microdissected hippocampus. Briefly, 5 μg protein samples were loaded with 5x loading buffer onto 12% SDS-PAGE gels with 4M urea, heated at 40°C for 10 min, and separated for 1.5 hrs at 100V. Samples were then transferred onto nitrocellulose membrane, incubated with rabbit anti-AQP4 antibodies (1:2500, Chemicon AB3594) in 5% milk/TBST overnight at 4°C. Next day, membranes were washed 3× 5 min in TBST, incubated with HRP-conjugated goat anti-rabbit IgG (1:7500, Chemicon) in TBST for 2 hrs. Sample loading was confirmed through detection of β-actin with mouse anti-β-actin (1:5000, Calbiochem, San Diego, CA). Bands were visualized with ECL and captured on Hyblot film (Denville Scientific Inc., Metuchen, NJ). Relative intensities of bands were obtained with the gel analysis function of ImageJ (NIH).

Quantitation of immunoreactivity

For immunoreactivity quantitation, white and black reference images were obtained, and a square box the width of the pyramidal cell layer was placed in each lamina to measure the average gray value for strata oriens, pyramidale, radiatum, lacunosum-moleculare, dentate molecular layer, dentate granule cell layer and the dentate hilus in individual hippocampi at each developmental time point (P9, 3 weeks, 6 weeks) (n=8 hippocampi analyzed per time point). Since the P9 stratum pyramidale was least immunoreactive of all laminae, results are presented as percent difference in gray value compared with P9 stratum pyramidale. Data were analyzed by ANOVA with post-hoc Bonferroni correction.

Patch clamp recording

To determine the expression of $K_{ir}4.1$ and AQP4 by NG2 cells and astrocytes, patch clamp analysis of morphologically identified fluorescent cells in the CA1 region of transgenic hGFAP-EGFP mice was performed, followed by cytoplasm harvest and RT-PCR analysis. Pyramidal neurons were used as controls. Briefly, transgenic hGFAP/EGFP mice of postnatal days P9-P12 were anesthetized, sacrificed by decapitation and their brains were dissected, washed and the hemispheres were cut into 300 m slices in frontal orientation using a vibratome (Leica Microsystems VT 1000S, Wetzlar, Germany). Slices were prepared and stored at 6°C in Ca^{2+}-free HEPES-buffered external solution. Acutely isolated cells were obtained from slices after protease treatment as previously described (Matthias et al., 2003).

Membrane currents were measured with the patch-clamp technique in the whole-cell configuration. Currents were amplified (EPC-7, HEKA elektronik, Lambrecht, Germany), filtered at 3 and 10 kHz and sampled at 10 and 100 kHz by an interface connected to a computer system, which also served as a stimulus generator. The resistance of the patch pipettes was 4 M (borosilicate glass; Malsfeld, Hilgenberg, Germany). Capacitance and series resistance compensation (40-50%) were used to improve voltage clamp control. The bath solution contained (in mM): 150 NaCl, 5 KCl, 2 $MgCl_2$, 2 $CaCl_2$, 10 HEPES and 10 glucose (pH 7.4). The pipette solution was composed of (in mM): 130 KCl, 0.5 $CaCl_2$, 2 $MgCl_2$, 5 BAPTA, 10 HEPES and 3 Na_2-ATP (pH 7.25). Recordings were obtained at room temperature. All reagents were purchased from Sigma (Taufkirchen, Germany) unless otherwise stated.

Single-cell RT-PCR analysis

Single-cell transcript analysis was performed as previously described (Matthias et al., 2003). Briefly, after recording of isolated cells, the cell at the tip of the pipette was transferred to a separate dish to be washed with fresh bath solution. The cell was aspirated into the recording pipette under microscopic control, and the cell content and ~3 μl of the pipette solution were expelled into a reaction tube containing 3 μl DEPC-treated water. The reaction tube was frozen and stored at –80 °C. RT was performed in a solution containing first strand buffer (Invitrogen, Karlsruhe, Germany), dithiothreitol (DTT, 10 mM), dNTPs (4×250 μM; Applied Biosystems, Darmstadt, Germany), RNasin™ (20 U; Promega, Mannheim, Germany), random hexamer primers (50 μM; Roche, Mannheim, Germany), and reverse transcriptase (SuperscriptIII, 100 U, Invitrogen) at 37 °C for 1 hr. A multiplex two-rou nd single-cell PCR was performed with primers for Kir4.1 and AQP4 (Table 1). The first PCR was performed after adding PCR buffer, $MgCl_2$ (2.5 mM) and primers (200 nM each) to the RT product (final volume 50 μl). After denaturation, 5 U *Taq* polymerase (Invitrogen, Karlsruhe, Germany) was added. Thirty-five cycles were performed (denaturation at 94 °C, 25 s; annealing at 51 °C, 2 min for the first 5 cycles, and 45 s for the remaining cycles; extension at 72 °C, 25 s; final elongation at 72 °C, 7 min). An aliquot (2 μl) of the PCR product was used as template for the second PCR (25 cycles; annealing at 54 °C, first 5 cycles: 2 min, remaining cycles: 45 s) using nested primers (Table 1). The conditions were the same as described for the first round, but dNTPs (4×50 μM) and Platinum *Taq* polymerase (2.5 U; Invitrogen) were added. Products were identified with gel electrophoresis using a molecular weight marker (φ×174 *Hinc*II digest, Eurogentec, Seraing, Belgium). As a positive control, RT-PCR for single cells and for total RNA from mouse brain were run in parallel. Negative controls were performed using distilled water or bath solution for RT-PCR. After omitting the reverse transcriptase, no PCR product was observed.

RESULTS

Developmental regulation of AQP4 in the mouse hippocampus

AQP4 was developmentally regulated in the mouse hippocampus, with gradually increasing expression from P9 through 3 weeks and 6 weeks (Figure 1, Figure 3B). At P9, hippocampal AQP4 immunoreactivity was strongest along the hippocampal fissure and in the SLM of CA1 and was also diffusely expressed on blood vessels (glial endfeet) throughout the hippocampus. As development proceeded at 3-weeks and 6-weeks time points, increasing AQP4 immunoreactivity was observed throughout the hippocampus. In particular, at 3 weeks stronger expression compared to P9 was seen in the dentate hilus and CA1. The expression pattern appeared to be on astrocytic processes within the neuropil, forming bush-like networks of immunoreactivity. By 6 weeks (young adult mice), increased and more diffuse parenchymal immunoreactivity of AQP4 was observed. No specific immunoreactivity was present with our sensitive immunohistochemical assay in sections from adult AQP4$^{-/-}$ mice (Figure 1, *right*). Western blot analysis confirmed developmental upregulation of AQP4. We conducted Western blot analysis of microdissected hippocampal homogenates from P9, 3-week and 6-week time points. As with the immunohistochemical analysis, Western blot demonstrated a developmental upregulation of hippocampal AQP4 protein expression (Figure 2). One-way ANOVA demonstrated significance ($p<0.05$) and *post-hoc* Bonferroni tests confirmed significant differences between P9 and 6 weeks ($p<0.01$) and 3 weeks and 6 weeks ($p<0.05$).

Laminar-specific expression of AQP4

At all developmental time points, the expression pattern of AQP4 within the hippocampus was laminar-specific (Figure 1, Figure 3B). Even in the young adult (6-week-old hippocampus), marked laminar specificity of parenchymal AQP4 immunoreactivity was consistently observed (Figure 3A). While there was never any laminar specificity of blood vessel AQP4 immunoreactivity, high expression of AQP4 was found within the CA1 SLM and the ML of the DG (Figure 3B). A clear difference was consistently observed between the CA1 SLM and CA1 stratum radiatum (SR), with stronger AQP4 immunoreactivity in the former (Figure 3, Figure 4). Less intense immunoreactivity was observed in CA1 stratum oriens (SO), CA1 stratum pyramidale (SP), dentate granule cell layer (DGC) and the hilus (H) of the DG (Figure 3B). Interestingly, the subgranular zone of the DG displayed a thin layer of AQP4 immunoreactivity. Within these layers, AQP4 immunoreactivity was found as a diffuse pattern of process staining. AQP4 immunoreactivity was also found on blood vessels (presumably on astrocytic endfeet ensheathing blood vessels, see Figure 5). The expression by endfoot/blood vessel of AQP4 immunoreactivity appeared to be uniform across the layers of the hippocampus.

Co-expression of AQP4 with glial and neuronal markers

In order to characterize the cell-type specificity of AQP4 expression, we performed double-label immunohistochemistry with the astroglial markers GFAP and S100β. We found throughout the hippocampus that AQP4-positive cells were GFAP-positive, confirming that AQP4 is found on astrocytes. Many AQP4/GFAP-positive cells were found in CA1 SLM, and these cells possessed the morphology of *bona fide* protoplasmic astrocytes (Figure 4). In contrast, high resolution confocal analysis was often necessary to reveal faint AQP4 immunoreactivity of GFAP-positive cells in the CA1 SR (Figure 4). In all cases, AQP4 immunoreactivity appeared on the cell surface and not within the cytoplasm, and was less intense than at blood vessels. S100β, another marker of cells with astroglial properties in the hippocampus (Hinterkeuser et al., 2000,Ogata and Kosaka, 2002,Matthias et al., 2003) also abundantly co-localized with AQP4 (Figure 5).

NG2 cells, a distinct group of CNS glia characterized by surface expression of the NG2 protein sharing many properties with GluR or complex glial cells (Bergles et al.), expressed only marginal levels of AQP4 if any (Figure 6).

AQP4 was not found to colocalize with the neuronal marker NeuN in any of the hippocampal laminae (Figure 7). Dense NeuN immunoreactivity was found, as expected, in the principal neuronal cell layers of the hippocampus (DGC and CA1 SP). AQP4 was found predominantly in the endfeet of blood vessels penetrating through these principal cell layers, but not in close proximity to the neuron cell bodies.

Single cell RT-PCR analysis

To investigate AQP4 expression at the single cell transcript level, multiplex single-cell RT-PCR was performed using primers also recognizing transcripts encoding $K_{ir}4.1$ (Schröder et al., 2002, Seifert et al., 2009). For cell identification, we took advantage of transgenic hGFAP/EGFP mice conferring fluorescence to living cells with GFAP promoter activity (Matthias et al., 2003). Freshly isolated astrocytes were selected according to the morphological and functional criteria as reported. After patch clamp recording and pharmacological analysis, the cytoplasm of the respective cell was harvested and RT-PCR was conducted, revealing co-expression of AQP4 and $K_{ir}4.1$ mRNA in all cells tested (n = 11; Figure 8A, B). In addition to astrocytes, NG2 cells are fluorescently labelled in hGFAP/EGFP mice (Matthias et al., 2003). Extending analysis to NG2 cells, AQP4 mRNA was encountered in the majority of these cells (n = 12 of 13 cells; 92%), with most cells co-expressing $K_{ir}4.1$ mRNA (n = 7; 58%; Figure 8C).

Expression of $K_{ir}4.1$ in $AQP4^{-/-}$ mice and AQP4 in $K_{ir}4.1^{-/-}$ mice

Previous studies indicated subcellular co-localization of AQP4 with the inwardly rectifying potassium channel $K_{ir}4.1$ both by electron micrographic and coimmunoprecipitation analyses (Connors et al., 2004, Nagelhus et al., 2004). Our RT-PCR results (above) suggest cellular co-expression of AQP4 and $K_{ir}4.1$ by classical (GluT) astrocytes. To test for a potential interaction between AQP4 and $K_{ir}4.1$, we performed immunohistochemistry for AQP4 and $K_{ir}4.1$ in sections from mice with a deletion of $K_{ir}4.1$ and AQP4, respectively. In WT adult mouse hippocampus, $K_{ir}4.1$ immunoreactivity was found in a characteristic diffuse pattern with strong immunoreactivity in the neuropil surrounding neurons of CA3 and CA1, a distinct pattern from AQP4 immunoreactivity (Figure 9A). We noted abundant $K_{ir}4.1$ immunoreactivity in sections from $AQP4^{-/-}$ mice (Figure 9B). Similarly, robust AQP4 immunoreactivity was present in $K_{ir}4.1^{-/-}$ mice at P9 (Figure 9D). Together these results indicate that deletion of AQP4 or $K_{ir}4.1$ has no dramatic effects on $K_{ir}4.1$ or AQP4 immunoreactivity, respectively.

DISCUSSION

In this study we provide the first data on the developmental regulation of AQP4 expression in the hippocampus. In addition, we report a marked laminar pattern of AQP4 expression, with strongest immunoreactivity occurring in the SLM of CA1 and the ML of the DG. As expected, AQP4 colocalizes with the astroglial markers GFAP and S100ß. In contrast, AQP4 protein was almost absent in NG2 cells and never encopuntered in neurons. Postrecording single-cell RT-PCR analysis demonstrates that AQP4 and $K_{ir}4.1$ transcripts are co-expressed in both astrocytes and NG2 glia. We also report that genetic deletion of AQP4 or Kir4.1 does not drastically affect expression of Kir4.1 and AQP4, respectively.

Early immunogold studies of AQP4 expression in the brain showed an enrichment of AQP4 in endfeet membranes in contact with brain microvessels or subarachnoid space and a low

but significant concentration in non-endfeet membranes, including astrocyte membranes ensheathing glutamatergic synapses (Nielsen et al., 1997). In addition, polarized AQP4 expression was found in brain astrocytes and retinal Müller cells (Nagelhus et al., 1998, Nagelhus et al., 2004). Diffuse AQP4 immunoreactivity was recently described in the hippocampus of 9-week-old rats (Kim et al., 2009). A detailed study of the ontogeny of AQP4 in the cerebellum (Wen et al., 1999) showed low levels of AQP4 in the first postnatal week and significant increases thereafter, similar to our current findings. However, in none of the previous studies was there specific attention paid to the developmental regulation and laminar specificity of AQP4 in the hippocampus, a structure critical to learning and memory and also important in disease states such as epilepsy. Our results in the mouse hippocampus demonstrate marked developmental upregulation of AQP4 between the early postnatal period and the young adult period. Further studies are necessary to examine AQP4 expression in the aged hippocampus.

The laminar specificity of AQP4 expression is remarkable in that it implies that CA1 SLM and the dentate ML may be particularly important sites for water and K^+ regulation. These layers lie on either side of the hippocampal fissure, where the hippocampal blood vessels penetrate the hippocampus (Sievers et al., 1992). Interestingly, the development of the hippocampus involves the development of glial scaffolds on either side of the hippocampal fissure, and a specific transcription factor mutant has been identified in which the outer marginal zone (precursor of the CA1 SLM) and dentate marginal zone (precursor of the dentate ML) selectively fail to develop normally (Zhao et al., 2006). Taken together, our laminar and cell-type specificity results suggest that the astrocytes of CA1 SLM and DG ML are distinct from other astrocytes in the hippocampus in expressing high levels of AQP4. Other studies have demonstrated morphological and functional differences between CA1 SLM and CA1 SR astrocytes (Wallraff et al., 2006). Our results thus contribute to the emerging concept of astrocyte heterogeneity (Matyash and Kettenmann, 2010).

Critical to the analysis of the role of AQP4 in the hippocampus is its cell type specificity. Distinct morphological and electrophysiological subtypes of cells with astroglial properties in the CA1 region of hippocampus have been described. Using transgenic mice expressing enhanced green fluorescent protein (EGFP) under the control of the human GFAP promoter (Nolte et al., 2001), in which astrocytes are fluorescently labeled, Matthias *et al*. (Matthias et al., 2003) distinguished two morphologically and functionally distinct EGFP-positive cell types. One, termed “GluT” cells, had the morphology of classical astrocytes and expressed glutamate transporters. The other, termed “GluR” cells, possessed different morphology and expressed ionotropic glutamate (AMPA) receptors. Further studies demonstrated that GluR cells display absence of gap junctional coupling (Wallraff et al., 2004) and receive synaptic input (Jabs et al., 2005), unlike astrocytes. GluR cells share many properties with NG2 cells although the degree of overlap between both populations has still to be clarified (Bergles et al., 2010). These studies have profound implications for the functional roles of these subgroups of hippocampal glial cells, in particular how they may respond to extracellular glutamate and in their roles in brain signaling (Mangin et al., 2008).

Our results indicate that AQP4 is expressed in astrocytes, as indicated by colocalization with GFAP and S100β and lacking or negligible colocalization with NG2 (Diers-Fenger et al., 2001) and NeuN. Interestingly, our RT-PCR data indicate that NG2 cells expressed AQP4 transcripts, but we never observed colocalization of AQP4 and NG2 at the protein level. Whether NG2 cells, which also express Kir channels (Schröder et al., 2002), contribute to K^+ buffering is unclear because these cells lacking gap junctional coupling (Wallraff et al., 2004). However, recent data demonstrated local redistribution of K^+ even in absence of astrocyte coupling (Wallraff et al., 2006). Hence, even in the absence of coupling, NG2 cells expressing $K_{ir}4.1$ and AQP4 at their processes might add to potassium buffering. High-

resolution morphological analysis is needed to clarify whether distant branches of NG2 cells contain AQP4 channels.

Early studies hypothesized functional interaction between AQP4 and $K_{ir}4.1$ based on subcellular colocalization in retinal Müller cells (Connors et al., 2004, Nagelhus et al., 2004) and previous *in vivo* data with AQP4$^{-/-}$ mice demonstrating markedly impaired K^+ clearance (Binder et al., 2006) which was in line with this hypothesis. $K_{ir}4.1$ is thought to contribute to K^+ reuptake and spatial K^+ buffering by glial cells, as pharmacological or genetic inactivation of $K_{ir}4.1$ leads to impairment of extracellular K^+ regulation (Ballanyi et al., 1987, Kofuji and Newman, 2004). However, while $K_{ir}4.1$ is known to be expressed in brain astrocytes and shows a similar developmental pattern as AQP4 (Higashi et al., 2001, Hibino et al., 2004, Seifert et al., 2009), two recent studies reported AQP4-independent Kir4.1 channel function (Ruiz-Ederra et al., 2007, Zhang and Verkman, 2008). Our current data support and extend these findings in showing that while AQP4 and $K_{ir}4.1$ are clearly co-expressed in identified glial cells by RT-PCR analysis, deletion of neither AQP4 nor $K_{ir}4.1$ markedly affects the macroscopic tissue distribution of the other protein.

In summary, the strikingly high expression of AQP4 in the CA1 SLM and DG ML identifies these hippocampal sublayers as potential sites of astrocytic K^+ and H_2O regulation. Hippocampal AQP4 expression is largely if not exclusively confined to astrocytes. These results begin to delineate the functional capabilities of hippocampal subregions and cell types for K^+ and H_2O homeostasis. Since both water (osmolality) (Andrew et al., 1989, Schwartzkroin et al., 1998) and extracellular potassium concentration (Yaari et al., 1986, Traynelis and Dingledine, 1988) have been shown to dramatically modulate neural excitability *in vivo*, further understanding of the glial modulation of ion and water homeostasis may lead to new concepts and targets for control of brain excitability.

Acknowledgments

This work was supported by a Van Wagenen Fellowship, American Association of Neurological Surgeons (DKB); BONFOR, DFG (SFB/TR3, TP C1; SE 774/3-1) and EU (FP7-202167 N*eur*oGLIA) grants (CS), a Mentored Clinical Scientist Research Career Development Award (K08 NS059674) (DKB) and an American Epilepsy Society/Milken Family Foundation Early Career Physician-Scientist Award (DKB). The authors are indebted to Alan Verkman and Paulo Kofuji for the provision of the AQP4$^{-/-}$ and Kir4.1$^{-/-}$ mice used in these studies.

REFERENCES

Amiry-Moghaddam M, Ottersen OP. The molecular basis of water transport in the brain. Nat Rev Neurosci 2003;4:991–1001. [PubMed: 14682361]

Amiry-Moghaddam M, Williamson A, Palomba M, Eid T, de Lanerolle NC, Nagelhus EA, Adams ME, Froehner SC, Agre P, Ottersen OP. Delayed K+ clearance associated with aquaporin-4 mislocalization: phenotypic defects in brains of alpha-syntrophin-null mice. Proc Natl Acad Sci U S A 2003;100:13615–13620. [PubMed: 14597704]

Andrew RD, Fagan M, Ballyk BA, Rosen AS. Seizure susceptibility and the osmotic state. Brain Res 1989;498:175–180. [PubMed: 2790471]

Badaut J, Ashwal S, Adami A, Tone B, Recker R, Spagnoli D, Ternon B, Obenaus A. Brain water mobility decreases after astrocytic aquaporin-4 inhibition using RNA interference. J Cereb Blood Flow Metab. 2010

Ballanyi K, Grafe P, ten Bruggencate G. Ion activities and potassium uptake mechanisms of glial cells in guinea-pig olfactory cortex slices. J Physiol 1987;382:159–174. [PubMed: 2442359]

Bergles DE, Jabs R, Steinhauser C. Neuron-glia synapses in the brain. Brain Res Rev 2010;63:130–137. [PubMed: 20018210]

Binder DK, Papadopoulos MC, Haggie PM, Verkman AS. In vivo measurement of brain extracellular space diffusion by cortical surface photobleaching. J Neurosci 2004;24:8049–8056. [PubMed: 15371505]

Binder DK, Yao X, Zador Z, Sick TJ, Verkman AS, Manley GT. Increased seizure duration and slowed potassium kinetics in mice lacking aquaporin-4 water channels. Glia 2006;53:631–636. [PubMed: 16470808]

Connors NC, Adams ME, Froehner SC, Kofuji P. The potassium channel Kir4.1 associates with the dystrophin-glycoprotein complex via alpha-syntrophin in glia. J Biol Chem 2004;279:28387–28392. [PubMed: 15102837]

Diers-Fenger M, Kirchhoff F, Kettenmann H, Levine JM, Trotter J. AN2/NG2 protein-expressing glial progenitor cells in the murine CNS: isolation, differentiation, and association with radial glia. Glia 2001;34:213–228. [PubMed: 11329183]

Frigeri A, Nicchia GP, Nico B, Quondamatteo F, Herken R, Roncali L, Svelto M. Aquaporin-4 deficiency in skeletal muscle and brain of dystrophic mdx mice. FASEB J 2001;15:90–98. [PubMed: 11149896]

Hibino H, Fujita A, Iwai K, Yamada M, Kurachi Y. Differential assembly of inwardly rectifying K+ channel subunits, Kir4.1 and Kir5.1, in brain astrocytes. J Biol Chem 2004;279:44065–44073. [PubMed: 15310750]

Higashi K, Fujita A, Inanobe A, Tanemoto M, Doi K, Kubo T, Kurachi Y. An inwardly rectifying K(+) channel, Kir4.1, expressed in astrocytes surrounds synapses and blood vessels in brain. Am J Physiol Cell Physiol 2001;281:C922–931. [PubMed: 11502569]

Hinterkeuser S, Schröder W, Hager G, Seifert G, Blümcke I, Elger CE, Schramm J, Steinhäuser C. Astrocytes in the hippocampus of patients with temporal lobe epilepsy display changes in potassium conductances. Eur J Neurosci 2000;12:2087–2096. [PubMed: 10886348]

Hsu MS, Lee DJ, Binder DK. Potential role of the glial water channel aquaporin-4 in epilepsy. Neuron glia biology 2007;3:287–297. [PubMed: 18634561]

Jabs R, Pivneva T, Hüttmann K, Wyczynski A, Nolte C, Kettenmann H, Steinhäuser C. Synaptic transmission onto hippocampal glial cells with hGFAP promoter activity. J Cell Sci 2005;118:3791–3803. [PubMed: 16076898]

Kim JE, Ryu HJ, Yeo SI, Seo CH, Lee BC, Choi IG, Kim DS, Kang TC. Differential expressions of aquaporin subtypes in astroglia in the hippocampus of chronic epileptic rats. Neuroscience 2009;163:781–789. [PubMed: 19619613]

Kofuji P, Ceelen P, Zahs KR, Surbeck LW, Lester HA, Newman EA. Genetic inactivation of an inwardly rectifying potassium channel (Kir4.1 subunit) in mice: phenotypic impact in retina. J Neurosci 2000;20:5733–5740. [PubMed: 10908613]

Kofuji P, Newman EA. Potassium buffering in the central nervous system. Neuroscience 2004;129:1045–1056. [PubMed: 15561419]

Ma T, Yang B, Gillespie A, Carlson EJ, Epstein CJ, Verkman AS. Generation and phenotype of a transgenic knockout mouse lacking the mercurial-insensitive water channel aquaporin-4. J Clin Invest 1997;100:957–962. [PubMed: 9276712]

Mangin JM, Kunze A, Chittajallu R, Gallo V. Satellite NG2 progenitor cells share common glutamatergic inputs with associated interneurons in the mouse dentate gyrus. J Neurosci 2008;28:7610–7623. [PubMed: 18650338]

Manley GT, Fujimura M, Ma T, Noshita N, Filiz F, Bollen AW, Chan P, Verkman AS. Aquaporin-4 deletion in mice reduces brain edema after acute water intoxication and ischemic stroke. Nat Med 2000;6:159–163. [PubMed: 10655103]

Matthias K, Kirchhoff F, Seifert G, Hüttmann K, Matyash M, Kettenmann H, Steinhäuser C. Segregated expression of AMPA-type glutamate receptors and glutamate transporters defines distinct astrocyte populations in the mouse hippocampus. J Neurosci 2003;23:1750–1758. [PubMed: 12629179]

Matyash V, Kettenmann H. Heterogeneity in astrocyte morphology and physiology. Brain Res Rev 2010;63:2–10. [PubMed: 20005253]

Nagelhus EA, Mathiisen TM, Ottersen OP. Aquaporin-4 in the central nervous system: cellular and subcellular distribution and coexpression with Kir4.1. Neuroscience 2004;129:905–913. [PubMed: 15561407]

Nagelhus EA, Veruki ML, Torp R, Haug FM, Laake JH, Nielsen S, Agre P, Ottersen OP. Aquaporin-4 water channel protein in the rat retina and optic nerve: polarized expression in Muller cells and fibrous astrocytes. J Neurosci 1998;18:2506–2519. [PubMed: 9502811]

Neely JD, Amiry-Moghaddam M, Ottersen OP, Froehner SC, Agre P, Adams ME. Syntrophin-dependent expression and localization of Aquaporin-4 water channel protein. Proc Natl Acad Sci U S A 2001;98:14108–14113. [PubMed: 11717465]

Nielsen S, Nagelhus EA, Amiry-Moghaddam M, Bourque C, Agre P, Ottersen OP. Specialized membrane domains for water transport in glial cells: high-resolution immunogold cytochemistry of aquaporin-4 in rat brain. J Neurosci 1997;17:171–180. [PubMed: 8987746]

Niermann H, Amiry-Moghaddam M, Holthoff K, Witte OW, Ottersen OP. A novel role of vasopressin in the brain: modulation of activity-dependent water flux in the neocortex. J Neurosci 2001;21:3045–3051. [PubMed: 11312289]

Nolte C, Matyash M, Pivneva T, Schipke CG, Ohlemeyer C, Hanisch UK, Kirchhoff F, Kettenmann H. GFAP promoter-controlled EGFP-expressing transgenic mice: a tool to visualize astrocytes and astrogliosis in living brain tissue. Glia 2001;33:72–86. [PubMed: 11169793]

Ogata K, Kosaka T. Structural and quantitative analysis of astrocytes in the mouse hippocampus. Neuroscience 2002;113:221–233. [PubMed: 12123700]

Papadopoulos MC, Manley GT, Krishna S, Verkman AS. Aquaporin-4 facilitates reabsorption of excess fluid in vasogenic brain edema. FASEB J 2004;18:1291–1293. [PubMed: 15208268]

Ruiz-Ederra J, Zhang H, Verkman AS. Evidence against functional interaction between aquaporin-4 water channels and Kir4.1 potassium channels in retinal Muller cells. J Biol Chem 2007;282:21866–21872. [PubMed: 17525153]

Schröder W, Seifert G, Hüttmann K, Hinterkeuser S, Steinhäuser C. AMPA receptor-mediated modulation of inward rectifier K+ channels in astrocytes of mouse hippocampus. Mol Cell Neurosci 2002;19:447–458. [PubMed: 11906215]

Schwartzkroin PA, Baraban SC, Hochman DW. Osmolarity, ionic flux, and changes in brain excitability. Epilepsy Res 1998;32:275–285. [PubMed: 9761327]

Seifert G, Huttmann K, Binder DK, Hartmann C, Wyczynski A, Neusch C, Steinhauser C. Analysis of astroglial K+ channel expression in the developing hippocampus reveals a predominant role of the Kir4.1 subunit. J Neurosci 2009;29:7474–7488. [PubMed: 19515915]

Sievers J, Hartmann D, Pehlemann FW, Berry M. Development of astroglial cells in the proliferative matrices, the granule cell layer, and the hippocampal fissure of the hamster dentate gyrus. J Comp Neurol 1992;320:1–32. [PubMed: 1401238]

Traynelis SF, Dingledine R. Potassium-induced spontaneous electrographic seizures in the rat hippocampal slice. J Neurophysiol 1988;59:259–276. [PubMed: 3343603]

Vajda Z, Pedersen M, Fuchtbauer EM, Wertz K, Stodkilde-Jorgensen H, Sulyok E, Doczi T, Neely JD, Agre P, Frokiaer J, Nielsen S. Delayed onset of brain edema and mislocalization of aquaporin-4 in dystrophin-null transgenic mice. Proc Natl Acad Sci U S A 2002;99:13131–13136. [PubMed: 12232046]

Verkman AS. More than just water channels: unexpected cellular roles of aquaporins. J Cell Sci 2005;118:3225–3232. [PubMed: 16079275]

Wallraff A, Köhling R, Heinemann U, Theis M, Willecke K, Steinhäuser C. The impact of astrocytic gap junctional coupling on potassium buffering in the hippocampus. J Neurosci 2006;26:5438–5447. [PubMed: 16707796]

Wallraff A, Odermatt B, Willecke K, Steinhäuser C. Distinct types of astroglial cells in the hippocampus differ in gap junction coupling. Glia 2004;48:36–43. [PubMed: 15326613]

Wen H, Nagelhus EA, Amiry-Moghaddam M, Agre P, Ottersen OP, Nielsen S. Ontogeny of water transport in rat brain: postnatal expression of the aquaporin-4 water channel. Eur J Neurosci 1999;11:935–945. [PubMed: 10103087]

Yaari Y, Konnerth A, Heinemann U. Nonsynaptic epileptogenesis in the mammalian hippocampus in vitro. II. Role of extracellular potassium. J Neurophysiol 1986;56:424–438. [PubMed: 3760929]

Yao X, Hrabetova S, Nicholson C, Manley GT. Aquaporin-4-deficient mice have increased extracellular space without tortuosity change. J Neurosci 2008;28:5460–5464. [PubMed: 18495879]

Zhang H, Verkman AS. Aquaporin-4 independent Kir4.1 K+ channel function in brain glial cells. Mol Cell Neurosci 2008;37:1–10. [PubMed: 17869537]

Zhao T, Kraemer N, Oldekamp J, Cankaya M, Szabo N, Conrad S, Skutella T, Alvarez-Bolado G. Emx2 in the developing hippocampal fissure region. Eur J Neurosci 2006;23:2895–2907. [PubMed: 16819978]

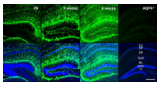

Figure 1. Developmental regulation of AQP4 immunoreactivity in mouse hippocampus

Low-power views of coronal mouse brain sections in P9 *vs.* 3-week-old *vs.* 6-week-old mice. While AQP4 immunoreactivity *(green)* is strongest in the CA1 SLM at P9, AQP4 immunoreactivity at 3 and 6 weeks is dramatically upregulated, particularly in CA1 SLM but also more diffusely throughout the hippocampus. Blood vessels are labeled well at all developmental stages. No specific immunoreactivity is present in sections from adult AQP4$^{-/-}$ mice (*right*). Nissl counterstains *(blue)* are shown in the bottom panels for each image. SO=stratum oriens; SP= stratum pyramidale; SR=stratum radiatum; SLM=stratum lacunosum moleculare; ML=molecular layer; DGC=dentate granule cell layer; H=hilus. Scale bar, 300 μm.

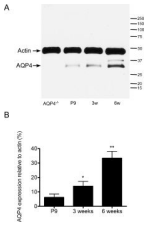

Figure 2. Western blot analysis of hippocampal AQP4 during development

A. Microdissected hippocampal homogenates were isolated from P9, 3-week, and 6-week-old WT mice and 6-week-old AQP4$^{-/-}$ mice and subjected to Western blot analysis for AQP4 and actin. Representative immunoblots demonstrate developmental regulation of AQP4 hippocampal protein levels (lower band, AQP4; upper band, actin loading control). B. Densitometric analysis demonstrates developmental upregulation of AQP4 expression from P9, 3-week, and 6-week samples (expressed as % actin expression) (n=3 per time point). *, $p<0.05$ compared to 6 weeks; **, $p<0.01$ compared to P9.

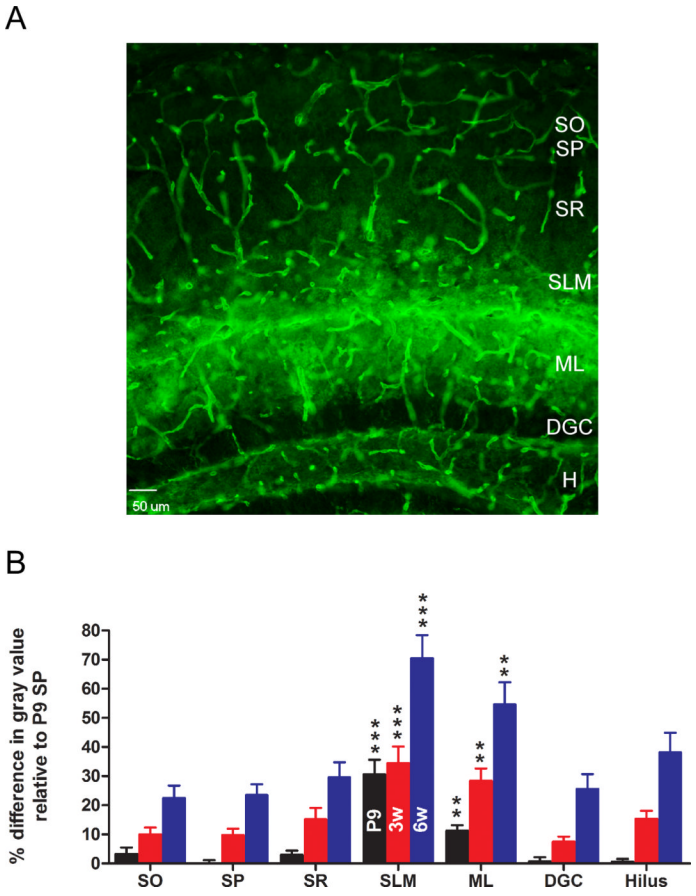

Figure 3. Laminar specificity of hippocampal AQP4 immunoreactivity

A. AQP4 immunoreactivity from 6-week-old mouse hippocampus demonstrates laminar specificity. While blood vessels are labeled well in all laminae, parenchymal AQP4 immunoreactivity is strongest in CA1 stratum lacunosum moleculare (SLM) and dentate gyrus molecular layer (ML) and along the hippocampal fissure separating these laminae. Laminar boundaries are derived from Nissl co-labeling (not shown for clarity). Scale bar, 50 μm. SO, stratum oriens; SP, stratum pyramidale; SR, stratum radiatum; DGC, dentate granule cell layer; H, hilus.

B. Developmental and laminar-specific quantitation of hippocampal AQP4 immunoreactivity. Values are expressed as % difference in gray value compared with P9 stratum pyramidale (SP) (see Materials and Methods). P9, black bars; 3 weeks, red bars; 6 weeks, blue bars. Higher values indicate more intense immunoreactivity. **, $p<0.01$ and ***, $p<0.001$ compared with SP at same time point.

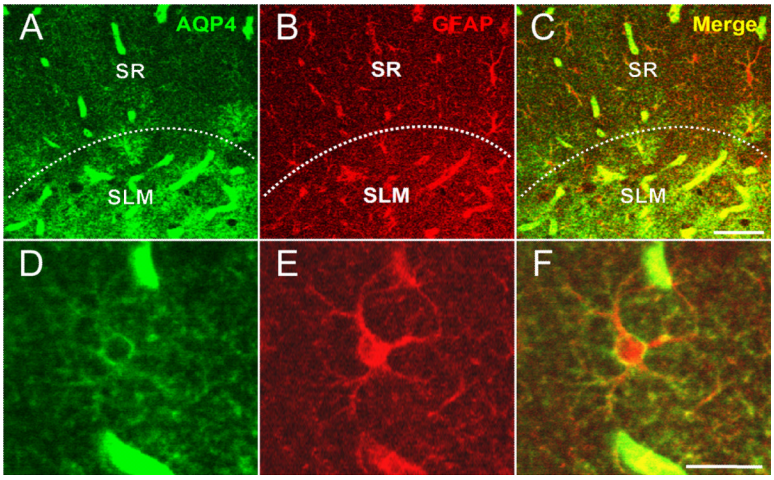

Figure 4. Colocalization of AQP4 and GFAP

Immunoreactivity for AQP4 (A), GFAP (B) and merged (C, F) is shown at the hippocampal CA1 SLM/SR border (dotted line) in a 3-week-old mouse. Note that in the SLM, there is significant colocalization of GFAP and AQP4 on cells with the morphology of *bona fide* astrocytes, whereas in the SR, GFAP-labeled astrocytes are seen that are AQP4-negative. AQP4 labels blood vessels in both layers. Higher-power images (D-F) demonstrate AQP4 and GFAP colocalization on an astrocyte in CA1 SR from a 6-week-old mouse. Scale bars, 50 μm (*top*), 20 μm (*bottom*).

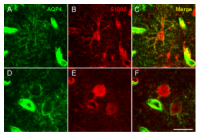

Figure 5. Colocalization of AQP4 and S100β

Immunoreactivity for AQP4 (A, D), S100β (B, E) and merged (C, F) is shown for two representative astrocytes in 3-week-old mouse CA1 SLM. In both panels, colocalization of AQP4 and S100β along the plasma membrane and processes can be observed. In one case (A-C), astrocyte morphology is clearly seen along with surrounding blood vessels. In the other case (D-F), colocalization of AQP4 and S100β is seen also in an astrocyte endfoot contacting a blood vessel. Scale bar, 20 μm.

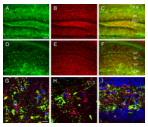

Figure 6. Marginal colocalization of AQP4 and NG2

Double-label immunoreactivity (C, F) for AQP4 (*green*, A, D) and NG-2 (*red*, B, E) is seen in DG (A-C) and CA1 (D-F) of the hippocampus. NG2-labeled cells appear throughout the hippocampus but mostly lack co-labeling with AQP4. Confocal images (G-I) from CA1 SR (G), DG ML (H) and DG hilus (I) demonstrate NG2-labeled cells (*red*) (Nissl, *blue*) and AQP4-labeled cells (*green*). SO=stratum oriens; SP= stratum pyramidale; SR=stratum radiatum; SLM=stratum lacunosum moleculare; ML=molecular layer; DGC=dentate granule cell layer; H=hilus. Scale bars: A-F, 100 μm, G-I 20 μm.

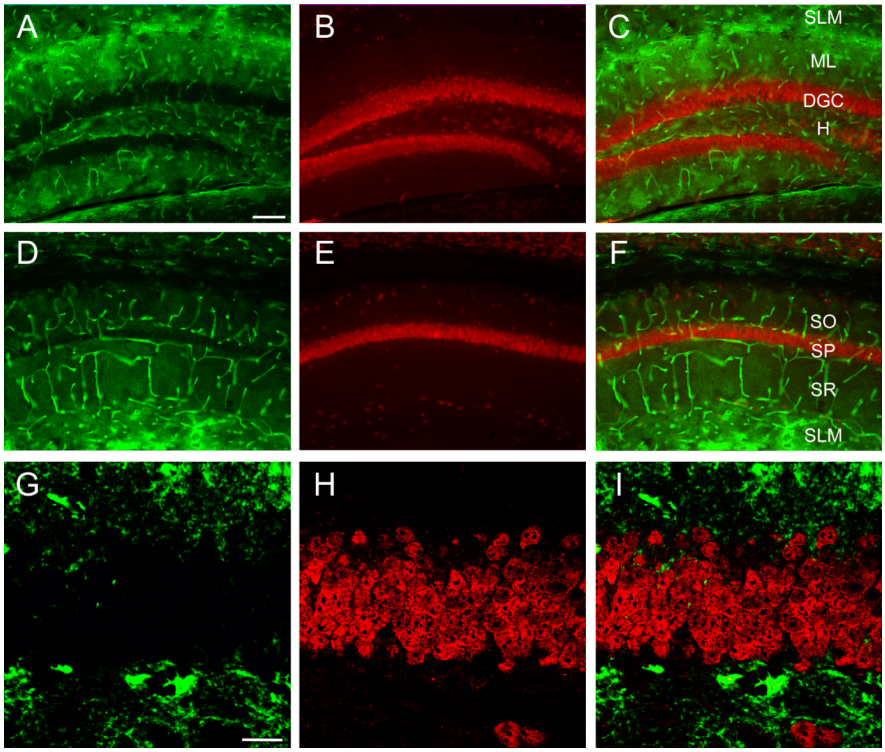

Figure 7. Lack of colocalization of AQP4 and NeuN

Double-label immunoreactivity (C, F) for AQP4 (*green*, A, D) and NeuN (*red*, B, E) is seen in DG (A-C) and CA1 (D-F) of the hippocampus. NeuN-labeled cells appear particularly in the principal cell layers throughout the hippocampus but are not co-labeled with AQP4. Confocal series from the DGC (G-I) shows NeuN-labeled granule cells but lack of colocalization of AQP4 and NeuN immunoreactivity. SO=stratum oriens; SP= stratum pyramidale; SR=stratum radiatum; SLM=stratum lacunosum moleculare; ML=molecular layer; DGC=dentate granule cell layer; H=hilus. Scale bars: A-F, 100 μm, G-I 20 μm.

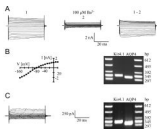

Figure 8. Co-expression of AQP4 and K_{ir}4.1 mRNA by identified hippocampal glial cells

A. A freshly isolated astrocyte was de- and hyperpolarized between +30 mV and -120 mV (10 mV increments; holding potential -60 mV; *left*). Then, the same protocol was applied after adding 100 μM $BaCl_2$ to the bath (*middle*); the *right* panel shows the Ba^{2+}-sensitive current.

B. I/V-relation of the Ba^{2+}-sensitive currents (*left*). Note that currents reversed close to the K^+ equilibrium potential (-82.3 mV). DNA gels demonstrate that the recorded cell co-expressed K_{ir}4.1 and AQP4 transcripts (*right*).

C. An NG2 cell was analyzed as described above (holding potential -70 mV; de- and hyperpolarization between +20 and -130 mV) (*left*). The cell also co-expressed AQP4 and K_{ir}4.1 mRNA (*right*).

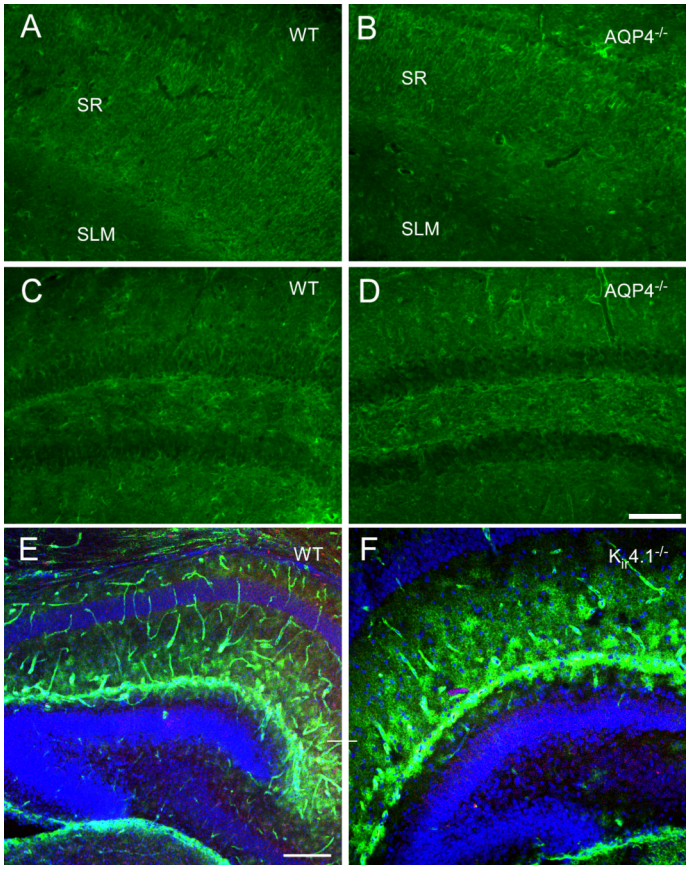

Figure 9. Deletion of AQP4 or K_{ir}4.1 does not dramatically affect K_{ir}4.1 or AQP4 immunoreactivity

K_{ir}4.1 immunoreactivity in adult hippocampus in WT (A, C) and AQP4-/- mice (B, D). Note the abundance of astrocytic process immunoreactivity in both CA1 (A, B) and dentate gyrus (C, D) in both genotypes. Apparently, CA1 stratum radiatum (sr) displays more intense immunoreactivity than CA1 stratum lacunosum moleculare (slm) in both genotypes (A, B). Scale bar, 100 μm.

AQP4 immunoreactivity in P9 hippocampus in WT (E) and Kir4.1-/- (F) mice. A similar pattern of AQP4 immunoreactivity is observed with blood vessel and parenchymal immunoreactivity indicating no dramatic effects of K_{ir}4.1 deletion on AQP4 immunoreactivity. Scale bar, 200 μm.

TABLE 1

Primers for single-cell rT-PCR

Gene	Sequence	Position	Product length	GeneBank Accession No.
$K_{ir}4.1$	se 5‘-TATCAGAGCAGCCACTTCACCTTC	-32	570 bp	NM_020269
	as 5‘-GGATCGTCTCGGCCCTCTTCTTAG	515		
$K_{ir}4.1$ (nested)	se 5‘-TTCACCTTCGAGCCAAGATGACG	-11	338 bp	
	as 5’-AGGCGTGTGGTTGGCAGGAG	302		
AQP4	se 5‘-AGCCGGCATCCTCTACCTG	387	427 bp	NM_009700
	as 5’-CTGCGCGGCTTTGCTGAA	796		
AQP4 (nested)	se 5‘-CTGGCCATGGGCTCCTGGTG	467	320 bp	
	as 5’-AAGGCGACGTTTGAGCTCCACATC	763		

‘Se’ and ‘as’ mark sense and antisense primers. Position 1 is the first nucleotide of the initiation codon. $K_{ir}4.1$ and AQP4 sense and antisense primers are located on different exons, respectively.